Transient voltages and energy balance in REBCO insulated magnet: experimental and numerical studies

Julien Vialle[1], Arnaud Badel[1,2], Blandine Rozier[1*], and Pascal Tixador[1]

[1] Université Grenoble Alpes, CNRS, Grenoble INP, G2Elab/Institut Néel, F-38000 Grenoble, France
[2] High Field Laboratory for Superconducting Materials, IMR, Tohoku University, Sendai 980-8577, Japan
[*]B. Rozier is now with Altair-France, F-38240 Meylan, France

E-mail: andre-julien.vialle@neel.cnrs.fr

Abstract

Different means are investigated today to protect a REBCO coil against local thermal runaway, what is commonly called a "Quench". Metal Insulated Coil or No-Insulated coil have been successfully introduced. However, these protections method may show other issues and are limited in terms of dynamics, making them impractical for fast applications. We successfully tested early detection of dissipative voltage followed by current dumping as a method to protect REBCO insulated test coils, even with engineering current density in the kA/mm2 range. Pick up coils can be used to compensate inductive coil voltage. In previous works we highlighted the presence of transient voltage due to the hysteretic current distribution in REBCO tape width, which can complicate the detection. We then developed a numerical electromagnetic model that reproduce the transient behaviour of REBCO coils. Here we study a small REBCO coil instrumented with three different pick-up coils, including a co-wound pick-up whose coupling is close to perfect. The post processing and analysis of the simulation results makes it possible to identify in the transient coil voltage the contribution due to transient losses and coil inductance variation. The resulting evaluation of the REBCO coil inductance and its variations is validated by analysis of the pick-up coil signals. From a practical point of view, this work shows the possibility to have very sensitive early detection of thermal runaway if the threshold is adjusted based on the expected coil compensated voltage drift. The interest of using isolated high-strength co-wound reinforcement tape as pick-up coil is also highlighted.

Keywords: Insulated REBCO magnet, current distribution, transient voltages, quench protection

1. Introduction and context

High-temperature superconducting materials enable coil designs with very high energy densities, because they transport large current density under high fields (more than 2000 A/mm² overall under 13 T at 4.2 K and still more than 1600 A/mm² under 21 T on short samples). They also have a very good mechanical strength (up to 600 MPa permissible longitudinal stress). Rare Earth–Barium–Copper Oxide (REBCO)-coated conductors are therefore widely studied for high field magnet applications.

However, ensuring their protection in case of a localized quench is still a challenge. Indeed, in LTS magnets, the resistive transition in general concerns a large volume of the magnet that can be quickly extended using quench heaters with limited energy. This is due to the small Minimum Quench Energy (MQE) and high Normal Zone Propagation Velocity (NZPV), in the 100 to 1000 cm/s. The quench leads to an abrupt voltage rise which makes it possible to clearly detect it, and trigger protection measures. In addition, since the dissipation extends throughout the magnet, the magnet quickly becomes resistive and the heating is evenly distributed. In REBCO magnet, there is strictly speaking no mass quench. This is due to their very high stability, with a minimum quench energy in the J to 10 J range [1], added to a much lower quench propagation speed, of barely a few centimetres per second [2].

For these reasons, if dissipation occurs in REBCO magnet, it is more likely due to local overstepping of the critical current, due either to intrinsic critical current inhomogeneity over the length of the superconducting REBCO tape, or a local damage in the winding. This will lead to local dissipations which if not detected can lead to destructive local thermal runaway also called hot spot. This hot spot problem is made even more severe by the very high current densities that can be used in REBCO coil designs. The detection of such local dissipation is difficult because the total resistive voltage remains small and its appearance may be hard to detect or easily confused with other contributions to the total coil voltage.

To prevent hot spots, different winding strategies have been proposed such as "no insulation" winding [3] or "metal as insulation" winding [4]. The great advantage of these two kinds of winding is that they are able to self-protect because the current can bypass the dissipative regions by transferring to the adjacent turns. This can even make it possible to dispense from any protection system [5, 6]. Nevertheless, even if these magnets offer a reliable operation, their longer charge and discharge times prevent their use for applications where the magnetic energy must be released quickly like SMES, while their larger magnetic field drift may be an issue for high field magnets where the stability and the quality of the field are desired.

For these reasons, developing safe conventionally insulated winding is a necessity. The method we favour is to use a classical protection method, rapid discharge of the coil in a dump resistor, but with a very sensitive detection system in order to have advance warning in case of thermal runaway.

1.1 Advantage of a low detection voltage threshold

As we mentioned above, the current density in REBCO coil can become very high (up to 1000 A/mm² on average) so the detection system must be made very sensitive to set keep dissipation minimum. In fact, the goal is to trigger the protection discharge before any thermal runaway occurs. Quench modelling studies [7, 8, 9] show that the discharge should occur before the dissipation exceed a few mV, even with modest current densities. It can be understood that for higher operating current densities the acceptable threshold value will decrease, so that the level of dissipation is kept low enough. Moreover, for a given current density, the added benefit of having a lower detection threshold is that the reaction delay can be longer and reach hundreds of milliseconds or even a few seconds. This time can be used for treating the voltage to avoid false positives (due to noise or turns movement).

1.2 Inductive voltage cancelation

This small hot spot detection voltage ranging from a few hundreds of µV to a few mV must be extracted from the voltage across the magnet. To get rid of the inductive component, one way is to have the voltages across two halves of the magnet equilibrated using a bridge. However, a hot spot voltage on one side might cover up another one happening on the other side completely or partly. This method may therefore underestimate the total dissipation, making it impossible to obtain reliable early detection. For this reason, we prefer to use the other classical method for inductive voltage cancelation: the use of a pickup coil (Fig. 1).

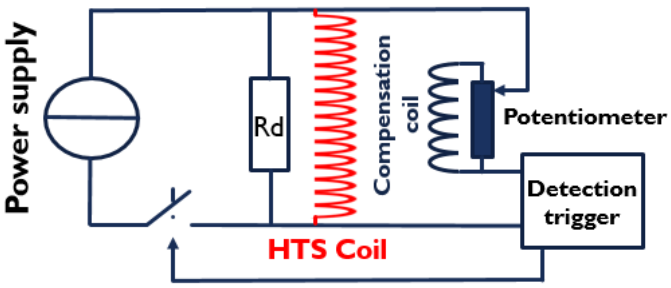

Figure 1. Electrical circuit to test our superconducting coils.

The size of the pick-up coil must be sufficient so that the magnetic flux it picks up induces a voltage equal or larger than that of the REBCO coil. enough to get the highest possible sensitivity. In order to minimize the pick-up coil size, it should be placed close to the superconducting coil (Fig. 2).

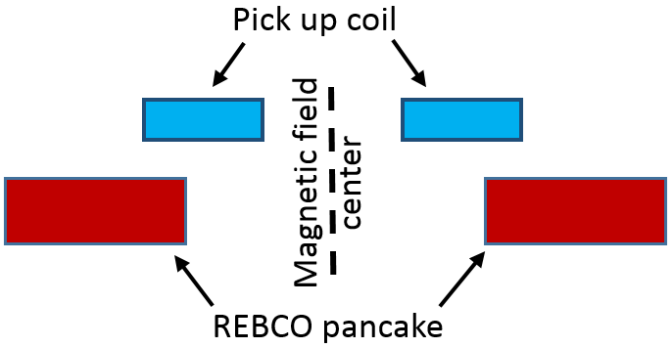

Figure 2. Magnetic coupling between a superconducting REBCO pancake and its pick up coil.

1.3 Compensated voltage drift

The challenge with such pick-up-based compensation is that the compensated voltage has transient component. If the bridge is adjusted to cancel out the REBCO coil inductive voltage at low level of current, the compensated signal *Vcomp* starts from zero but then "drifts" when the current increase (Fig. 3). This evolution of *Vcomp* is not caused by steady-state dissipation as the signal rapidly goes back to zero as soon as the current reaches a plateau, as it was already discussed in [10]. It must be noted that it is not visible when using a two-halves-bridge compensation as transient components exist on both sides and thus cancel each other.

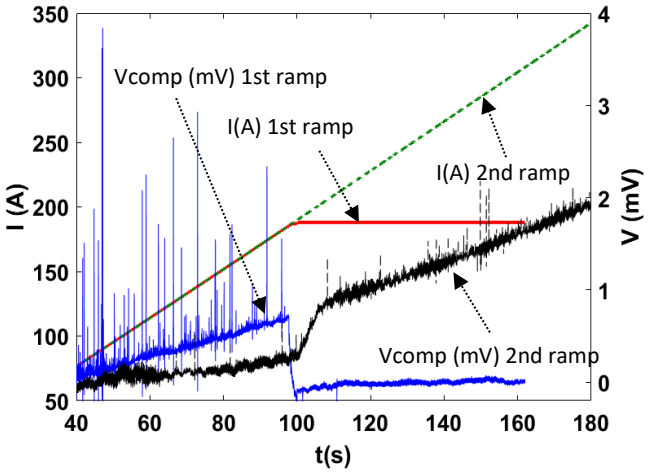

Figure 3. Dependence of the first and second (and following) current ramps on inductive voltage. The first current ramp in red and its compensated voltage in blue. The second current ramp in green dotted line and its compensated voltage in black.

That transient value of *Vcomp* can be up to an order of magnitude higher than our target detection threshold range, so it must be accounted for in the detection scheme. In order to better understand it, we developed a transient electromagnetic numerical model [11] making it possible to predict the variations of voltage across insulated REBCO coil during any current cycle, with or without background field, as well as the calculate of the transient field distribution.

1.4 Aim of this work

The aim of this paper is to develop a better understanding of the transient phenomena not only for the total voltage as studied in [11] but in terms of the different contributions to that voltage, either inductive or dissipative. For that we will establish the energy balance of the coil throughout charge and discharge cycles, and compare the modelling results with experimental data. The test coil is instrumented with the help of three different compensation coils to help discriminate the nature of the different contributions to the coil voltage experimentally. The first is a pick-up coil co-wound with the pancake to get a "perfect" magnetic coupling [12,13,14], in principle able to cancel completely the inductive component of the signal, the second one is a solenoidal pick-up coil close to the studied pancake with a partial coupling, and the last one is a Rogowski coil placed at the output of the current source and therefore fully magnetically decoupled. The paper is organized as follows.

First, the experimental setup will be described, as well as the numerical simulation input data and hypothesis. In a second part, the REBCO coil signals are studied. The model is used to establish the energy balance of the coil and a voltage decomposition is proposed to materialize the distinction that can be made between dissipative and inductive contributions to the transient coil voltage. This distinction is comforted in a third part by experimental results using the compensation coils. Then, an experimental ramping up to runaway is carried out on purpose to investigate protection enhancement.Finally, we will discuss other magnetic behaviors that we visualized on the experience and we will be able to conclude and talk about the perspectives.

2. Experimental and Numerical setup

2.1 REBCO coil design and experimental setup

The test coil is a single pancake (Fig. 4), which is wound with two tapes in parallel: an insulated REBCO tape (135 µm thick tape, from SuperOx) and a 30 µm thick *Durnomag*® tape. Both tapes are 6 mm wide. The superconducting tape is made of 60 µm of Hastelloy® C-276 substrate, with 17.5 µm of copper on both sides the tape, and 40 µm of polyamide insulation. The co-wound and REBCO pancake coils have 32 turns. The REBCO coil's current leads are a copper mandrel for the inner diameter and a copper crescent for the outer diameter as we can see on the figure 4. Both current leads are soldered at 180°C with InSn at SC pancake extremities. The main parameters of the REBCO coil are summarized in Tab. 1.

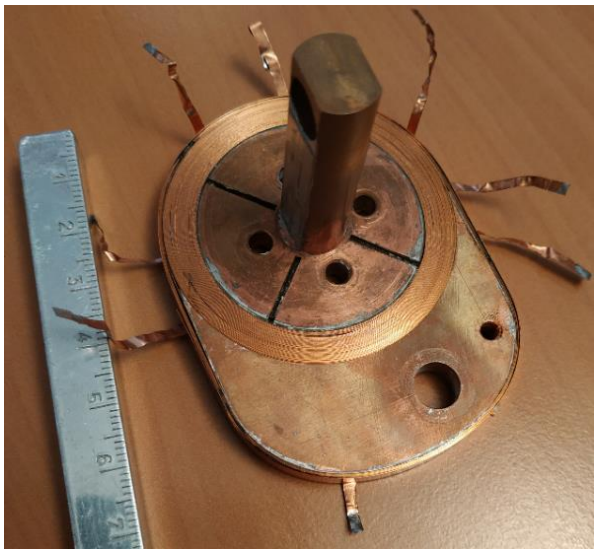

Figure 4. Single insulated REBCO pancake with a co-wound pick-up coil.

REBCO Coil and pick-up coils	
SuperOx Tape 6 mm wide 135 µm thick with Polyamide insulation. *Durnomag*® tape 6 mm wide 30 µm thick.	
I_c (77 K sf (100 µV/m)	210 A
32 turns	
Internal diameter	40 mm
Outer diameter	51 mm
Inductance	63.37 µH
Durnomag pick-up coil	32 turns
Copper pick-up coil	340 turns
Rogowski coil	2000 turns

Table 1 Single insulated REBCO pancake design and pick up coil turn number.

Voltage taps are placed on the copper current leads, the superconducting tape and the *Durnomag*® tape. In order to avoid over thicknesses inside the coil but also a critical current degradation, the voltages taps are made using a thin copper tape (0.05 mm thick and 2 mm wide), and are not soldered on the superconducting tape directly but wrapped around the REBCO tape and soldered on itself to form a loop, the winding tension ensuring the good contact between voltage tap and REBCO tape. The current source is controlled through a LabVIEW program. All voltage signals are acquired using a differential oscilloscope.

As mentioned previously we use pick up coils in order to get additional information on the coil behaviour, the goal being to differentiate the inductive and the dissipative parts of the coil voltage. For that the three pickup coil have different magnetic couplings.

The one obtained with the co-wound metallic tape is maximal, in the 0.97 to 0.99 range (see part 4). It is made by a co-wound *Durnomag*® tape alloy from Laminerie Mattthey S.A. Its properties are close to those of hastelloy, with a high resistivity (70 µOhm.cm) limiting the risk of eddy currents distorting the signal.

The second is a copper solenoid just below the magnet, with a coupling coefficient in the 0.362 to 0.358 range (see part 4), similar to what we could achieve in a real system.

The third one is a torus put on the external current lead (a Rogowski coil). With no coupling at all, it will give us an exact image of the current variation di/dt.

The whole system is schematically described Fig. 5

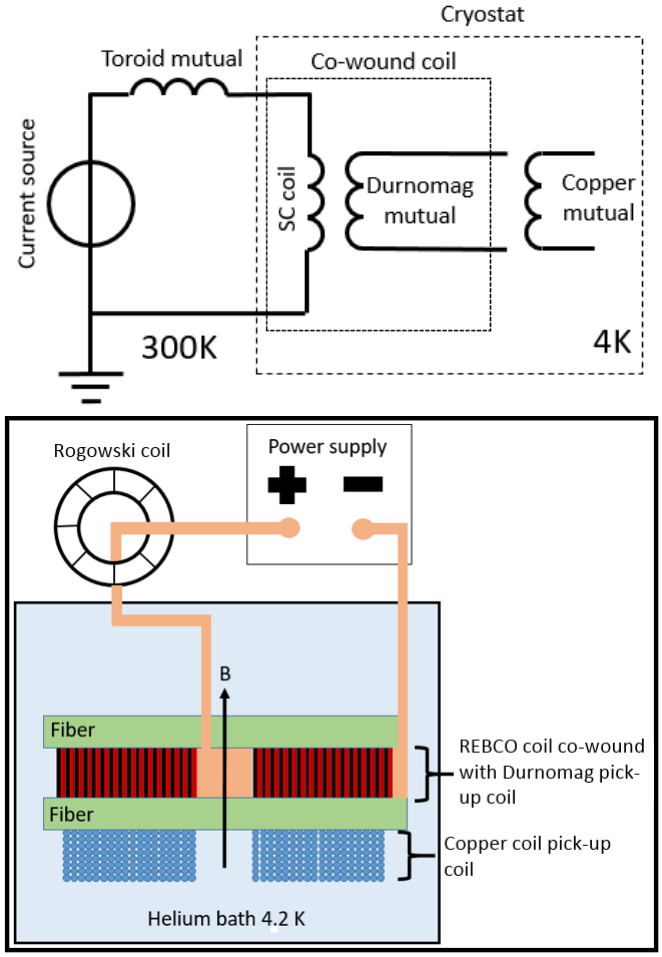

Figure 5. Electrical circuit (at the top) and a schematic of the experiment (at the bottom).

The experiments are all performed in liquid helium at 4.2 K, with no background field. In order to amplify phenomena due to the current distribution variation inside the superconducting tape, our tests are carried out with fast current ramps of 20 A/s to have large transient signals. Fast current ramps also minimize the influence of current leads heating. The discharge is even faster at 100 A/s to minimize burnout risk when ramping up to the critical current.

2.2 Numerical model definition and simulation parameters

We use the model presented in [11]. It is a transient two-dimensional (2D) axisymmetric model using a volume integral *J* formulation called MIPSE [15]. The E-J constitutive equation is a power law with an index value *n* of 25. We assume a constant *n* value because the impact of variations in realistic range is negligible. Trusting the temperature stability of our experimental setup, the temperature is assumed constant at 4.2 K.

The critical current density $Jc(B,\vartheta)$ then depends only on field amplitude and angle (Fig. 6). We use data from [16], relevant to the SuperOx REBCO conductor used in our experiment, with an adjustment coefficient applied to all data to adjust the surface to the properties of the tape actually used in our coil.

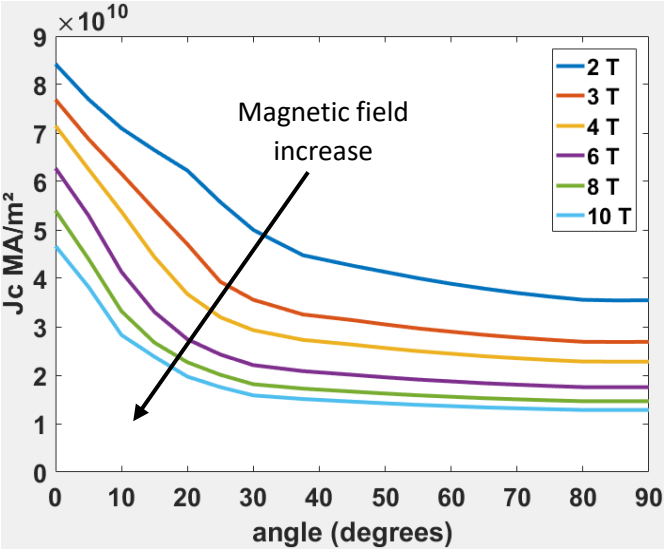

Figure 6. Reduced critical current versus angle for REBCO tape for different magnetic field.

The REBCO pancake is modelled based on the coil dimensions as measured after winding (Fig. 7). The turns of the coil are represented by line-segments corresponding to the tape width. Each turn is discretized in 50 elements. No current sharing between the conducting layers of the conductor is considered, the current flows through the superconducting layer only. That assumption is valid at low level of electric field where current sharing is negligible.

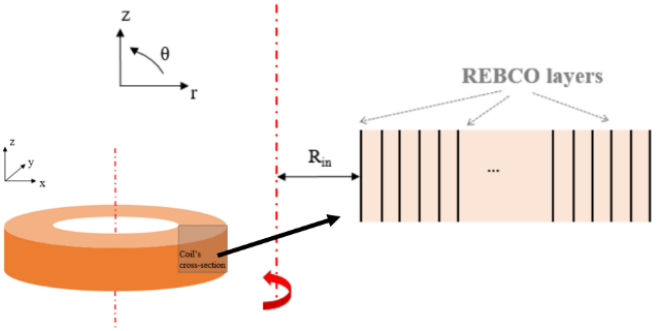

Figure 7. Simplified coil geometry represented in a 2D axisymmetric view.

The current cycle that we used for the simulations reproduce as well as possible the experimental considering simulation constrains. It consists of successive ramps to 500 A in 25 s., with a 5s plateau at the top and a very fast discharge (in 1 s). (Fig. 8).

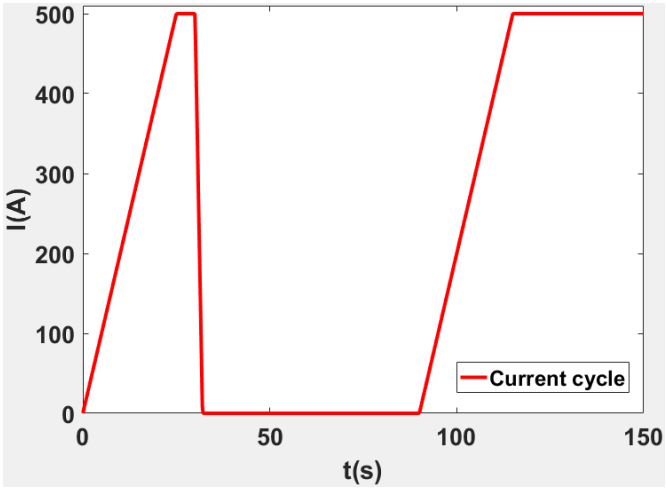

Figure 8. Current cycle for the experiment and the modelling.

The MIPSE integral formulation is very efficient in that only the active components, that is, the components where current is flowing, have to be meshed. In consequence the field is only calculated on the conductor. When for post-processing purpose we need to evaluate the field distribution around the coil, FEM axisymmetric magnetostatic simulation are conducted using COMSOL®. The local current densities calculated by MIPSE are imposed locally on the discretized conductor. This in particular allows us to evaluate the stored energy in the coil at any given moment.

3. Energy balance and transient voltages: comparison between modelling and experiments

In order to understand that behaviour, we developed in [11] a model to simulate the dynamic evolutions of the voltage across a REBCO coil (called V_{sc} for now on) during current

variations. It gave good estimation of the total voltage. This is also the case in this work.

During ramp up, the voltage drift is clearly visible as expected. It is not the same during the first ramp and during the following ones. Fig. 9, a non-linear variation of the experimental coil voltage for first ramp (in blue) and second ramp (in black) is clearly visible. When focusing on the voltage drift (Fig. 10), it is about 5 times higher during the first ramp than during the following ones. The pink dotted line on both Fig. 9 and 10 is the simulated value. As in [11], a coefficient was applied to all critical current values taken from [16] to get a good agreement with the experiment. This coefficient relates to the difference between the measured short sample performances and the performance of the length of conductor wound in the coil. It is 0.59 in this case.

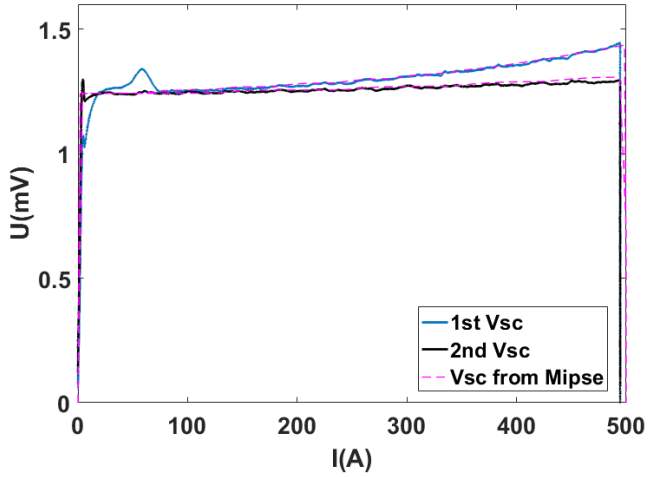

Figure 9. Coil voltage for an experimental first and second current ramp up to 500 A compared to the modelling results.

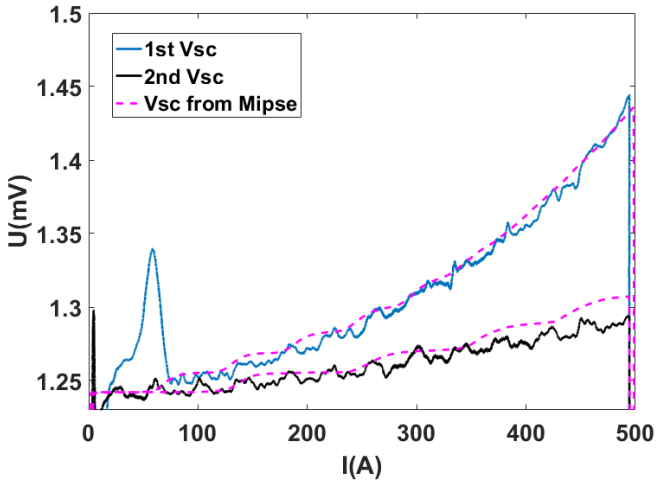

Figure 10. Zoom on the inductive voltage drift for an experimental first and second current ramp up to 500 A compared to the modelling results.

3.1 Decomposition of the voltage across a REBCO magnet during transient

Here we want to discuss how this voltage is composed.

A large part of it is naturally the inductive voltage, but the correct definition of an inductance for such a coil with a wide non-linear conductor is not straightforward. Let us consider $L_{ref\ magnet}$ the inductance of the coil for a homogeneous current distribution. It is a constant, even if it may vary slightly due to changes of the geometry if the electromagnetic forces are very high. The voltage related to it is then $L_{ref\ magnet}\frac{di_t}{dt}$.

In addition to that component, a transient voltage is due to the dynamic distribution of the current density in the conductor width when the coil current varies (and also if the background field varies). Intuitively, we can understand that it is related to the transient losses in the conductor, and thus represent a dissipation, let us call it $v_{trans.\ dissip}$. But the fact that the current redistributes in the conductor width means that the coil inductance is also changing, so that part of this voltage is inductive: let us call it $v_{trans.\ induc}$. We will define this two voltage component in part 3.3.1 and 3.3.2.

The voltage across the magnet v_{sc} can then be written as (1):

$$v_{sc} = L_{ref\ magnet}\frac{di_t}{dt} + v_{trans.\ induc} + v_{trans.\ dissip} + v_{defect} \quad (1)$$

i_t is the transport current.

With v_{defect} the voltage due to the local overstepping of the critical current: the component that we wish to detect.

$$v_{defect} = E_c \int_0^{\ell_{conductor}} \left(\frac{i_t}{I_c(l)}\right)^n dl \quad (2)$$

Where $\ell_{conductor}$ is the total length of the conductor used in the magnet.

In the next sections we will show that this decomposition of the signals has meaning and can be matched with experimental results. In this part, we want to validate quantitatively our decomposition of the REBCO coil voltage by establishing the energy balance of the coil in modelling and experiments.

3.2 Energy balance

Now that we have shown the good agreement between the modelling voltages and the experiment voltages, we focus on the energy exchanged, dissipated and stored and establish the energy balance.

3.2.1 Input energy.

The one thing accessible from both modelling and experiment is the power supplied from the source, whose integration gives the input Energy W_{in}.

$$W_{in} = \int_t v_{sc}.i_t \qquad (3)$$

Fig. 11 compares the energy supplied in the experiment for a first and a second current ramp with the supplied energy calculated from the model. Similarly, to the voltage case, the modelling results are in good agreement with the experimental results.

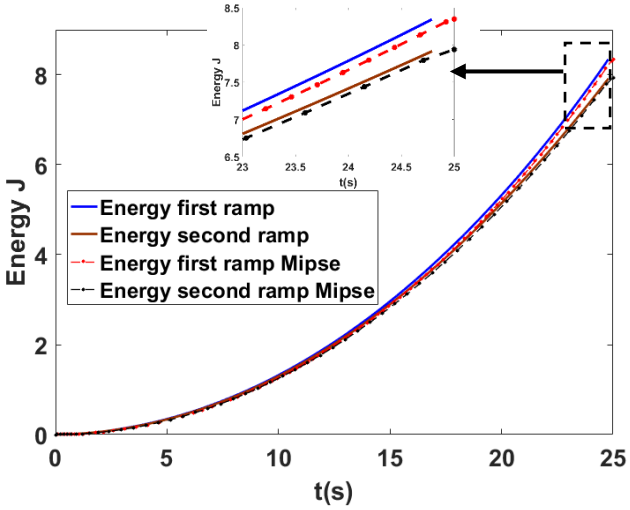

Figure 11. Energy transfer from the power supply for a first and a second current ramp up to 500 A.

One can notice the energy delta between the two ramps. It is related to dissipative losses, which are bigger for a first current ramp than for the following ones but also, to the magnetic hysteresis of the REBCO coil, as field is trapped after the first current cycle.

3.2.2 Losses modelling results

In the model we estimate the losses locally based on the local equivalent resistivity (ρ_{equ}). We can then integrate over the whole geometry to get the dissipating power using (4), with *n* the power Law index, *J* the local current density, and *Jc* the local critical current density.

$$Pac = \int_V \rho_{equ}.J^2 dV = Ec \int_v \left(\frac{J}{Jc}\right)^n .J\, dV \qquad (4)$$

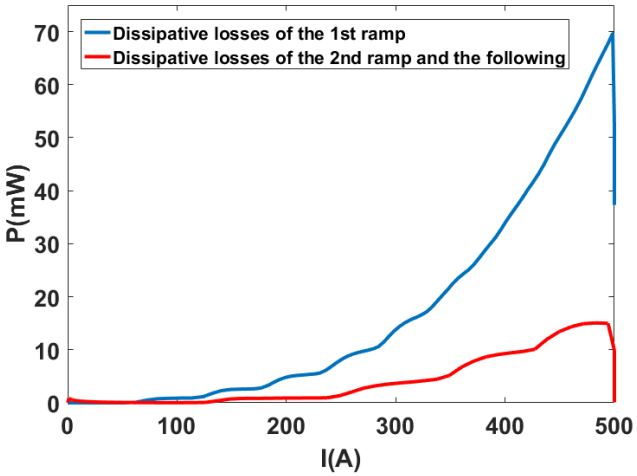

Figure 12. Dissipative losses for the first, then the second and the following ramps up to 500 A.

This calculated dissipation *Pac* is what is commonly called AC losses and are mostly hysteretic losses in our case with a single tape conductor. They correspond to all dissipative phenomena in a superconducting coil which occur during current or magnetic variations. These losses are represented Fig. 12. As can be expected, they are higher for a first ramp, from a magnetically virgin state, than for a second current ramp to the same current, by a factor of approximately 4.7.

3.2.3 Simulated stored energy

By integration of the losses over time we can then get the dissipated energy during the two current ramps. By subtracting that dissipated energy from the energy injected by the source, we obtain the energy stored in the coil (Fig. 13). That stored energy an also be obtained by integrating the field generated by the current distribution in the coil conductor at any given time, as explained in part 2.

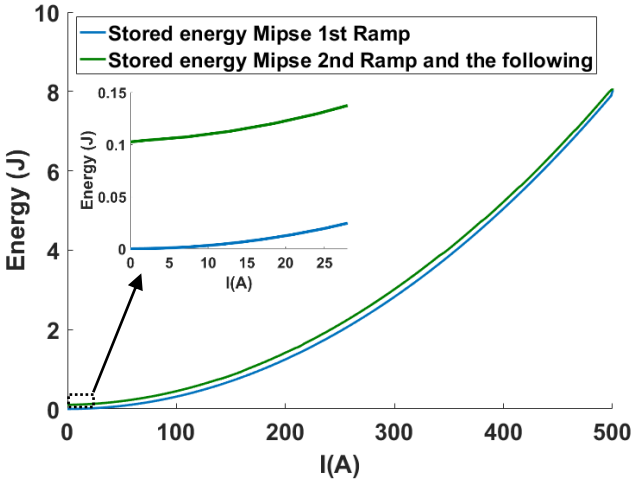

Figure 13. Stored energy for the first and the second (and following) current ramps.

3.2.4 Trapped field and trapped energy

Fig. 13 we can observe an offset to the stored energy at the beginning of the second ramp. It is due to the trapped field, which stores a small amount of energy.

Fig. 14 shows the field distribution at the beginning of the second ramp (at t = 90 s, with zero source current), which is the trapped field. The integration over the volume gives a trapped energy after one charge and discharge cycle of 100 mJ. That is the energy at the starting of the second ramp.

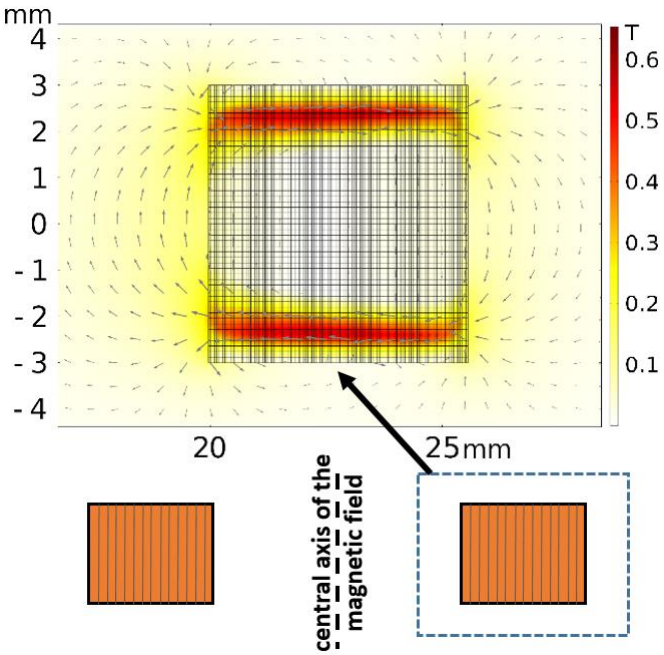

Figure 14. Trapped field and current distribution after one charge and discharge cycle. The arrows length corresponds to the log (B).

3.3 From energy balance to voltage components

3.3.1 Definition of coil inductance

As we said previously, precisely defining the inductance of a superconducting coil with a wide conductor (the REBCO tape) is not straightforward. Here we define an equivalent inductance L_{eq} for a given transport current I_t, related to the variation of the stored energy since the beginning of the ramp (5).

$$L_{eq}(I_t) = \frac{2(W_{mag}(I_t) - W_{mag}(0))}{{I_t}^2} \quad (5)$$

where $W_{mag}(I_t)$ is the energy stored in the magnetic field for a transport current I_t.

The interest of that definition is that it can be used for the first ramp but also for the following ramps, at the beginning of which the stored energy is not zero due to the trapped field.

Fig. 15 summarizes the evolution of that equivalent inductance during the first (in black) and following (in blue) ramps of current.

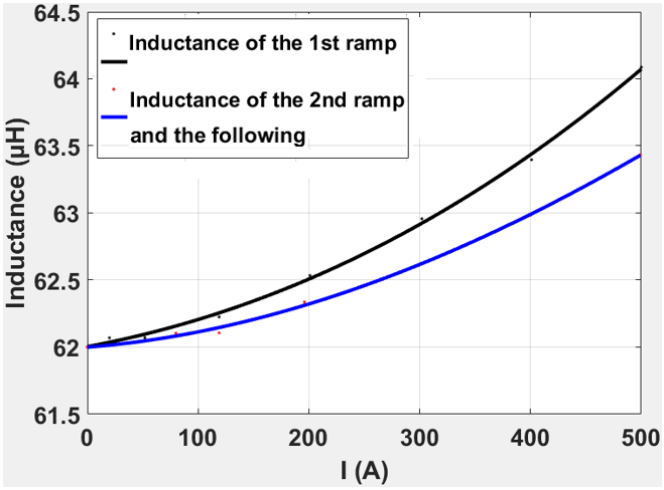

Figure 15. Equivalent inductance definition based on the energy versus the time.

The rising trend of the inductance with current was expected. In this self-field coil configuration, the current is concentrated on the edges of the REBCO tape and gradually penetrates toward the center while the transport current rises (Fig. 16). This behaviour increases the REBCO coil inductance.

Moreover, for the same current the equivalent inductance is smaller for the second current ramp (and following) than for the first. This can be understood: when reaching the maximum current $I_{t\,max}$ (here 500 A), the current density distribution and the magnetic stored energy $W(I_{t\,max})$ are the same for all the ramps, but for the second ramp (and following) there is a non-zero stored energy at the beginning, so that the energy variation during the ramp is smaller than for the first ramp.

The first ramp is unique, with higher losses and part of the energy trapped, so the inductance defined for that first ramp is not meaningful. It does not represent the usual behaviour of the coil in operation, which usually consist in many ramps without warming up. During the second ramp and the following ramps, the initial inductance and its variation will stay the same.

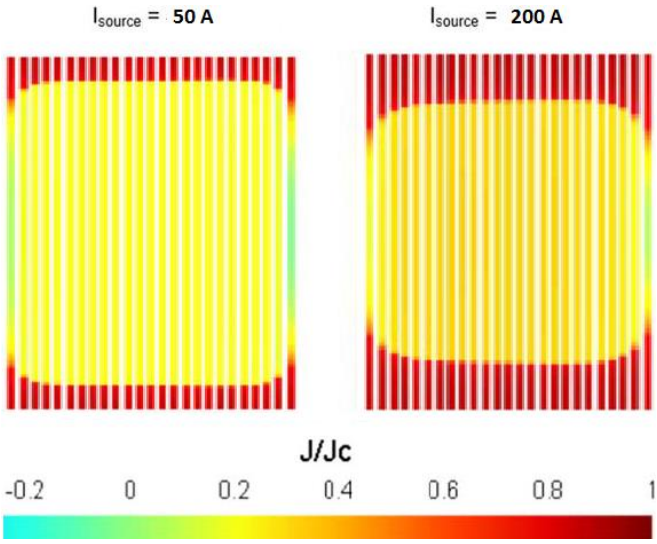

Figure 16. Normalized current density distribution along the tape width for 50 A and 200 A

The inductance drift confirms our assumption from part 2: not all of the coil voltage drift is due to dissipation, some of it is inductive. If we regroup the inductive components of the coil voltage, (1) can be rewritten as follows:

$$v_{sc} = v_{inductance} + v_{trans.\ dissip} + v_{defect} \quad (6)$$

with

$$v_{inductance} = L_{ref\ magnet}\frac{di_t}{dt} + v_{trans.\ induc} = L_{eq}(t)\frac{di_t}{dt} \quad (7)$$

3.3.2 Decomposition of the coil voltage

We can now subtract $v_{inductance}$ from the total coil voltage to evaluate the voltage component representing the transient losses, which we referred previously as $v_{trans.\ dissip}$. The result is shown Fig. 17 and Fig. 18 for the first and second ramps respectively.

The largest contribution to the coil voltage drift comes from that dissipative component. It represents about 79 % of the total voltage drift for the first ramp, and 62 % for the second and following. Note that the steps on the curves are due to the discretization of the conductor width in the model. Dotted lines are added to visualize the trends.

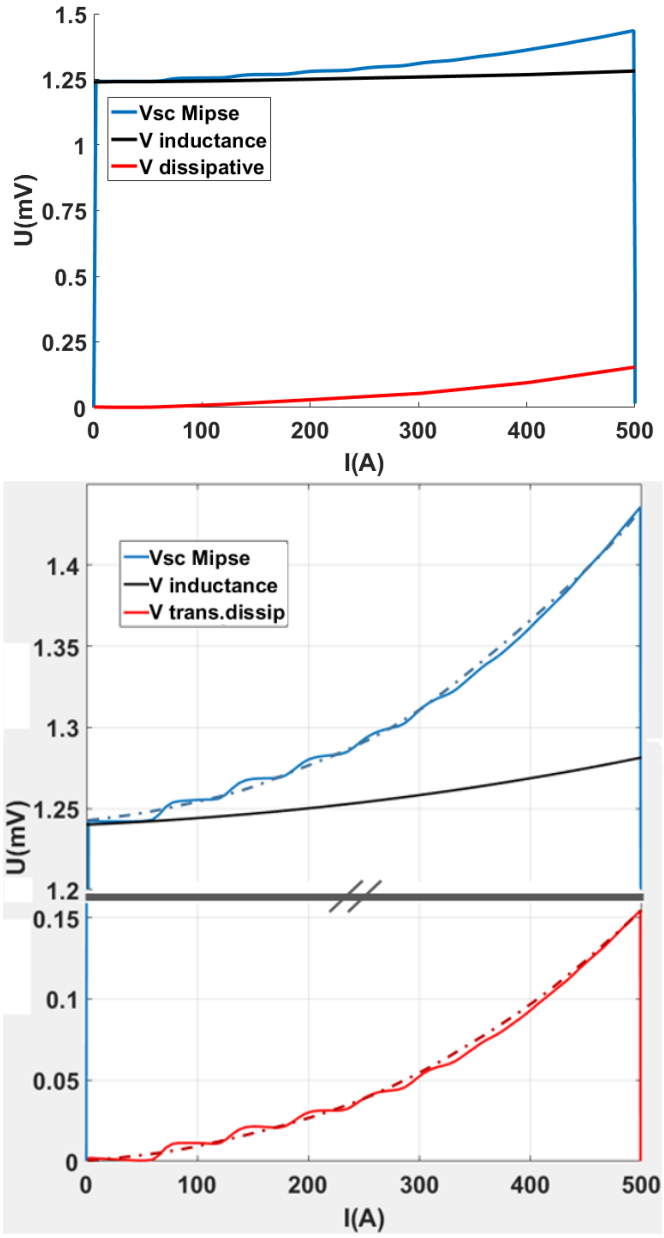

Figure 17. Calculated voltages contribution for the first current ramp. The dotted lines are there to help visualize the trend of the curve.

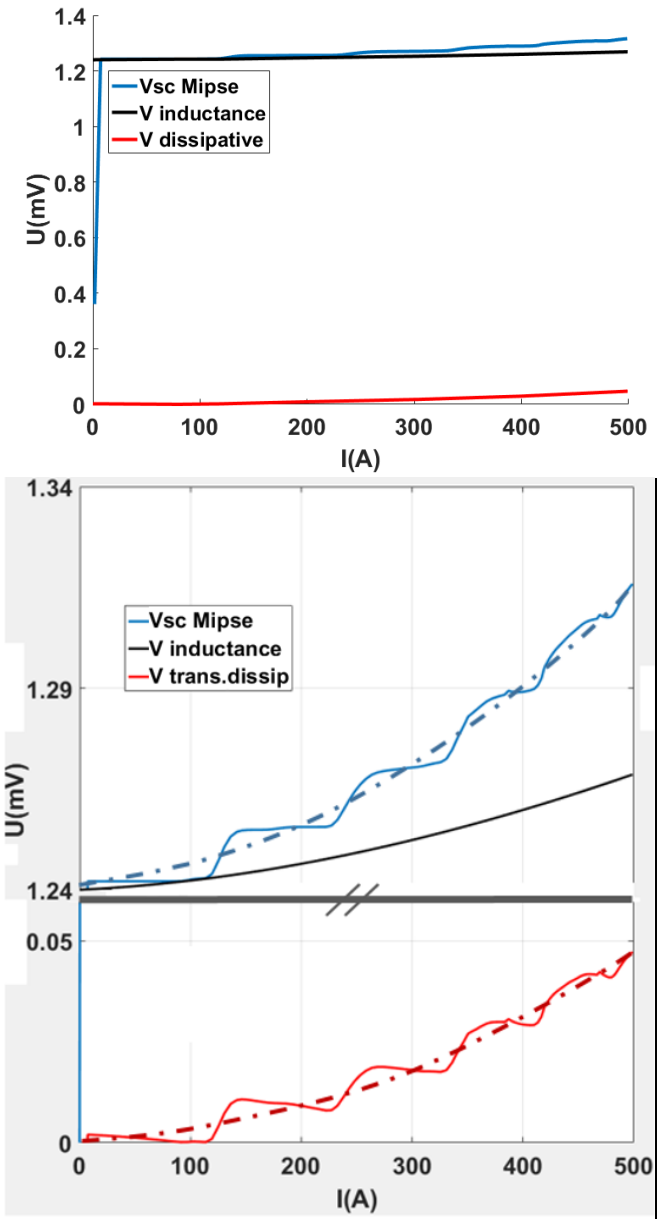

Figure 18. Calculated voltages contribution for the second and the following current ramps. The dotted lines are there to help visualize the trend of the curve.

3.3.2 Field hysteresis

As we saw previously in the figure 5 the model makes it possible to estimate the current density distribution inside each turns of the REBCO coil. With this information we can calculate the axial center magnetic field (B_{center}) generated by the coil and the magnetic field error (B_{error}) that corresponds to the difference between B_{center} value and the theoretical value if the current density was homogeneous ($B_{homogeneous}$).

$$B_{error} = B_{center} - B_{homogeneous} \quad (8)$$

Fig. 19 present the B_{error}-I curve calculated for the studied scenario, that is to say two current cycles up to 500 A. The curve does not follow the same path during the first cycle and the second, the trapped field being clearly visible.

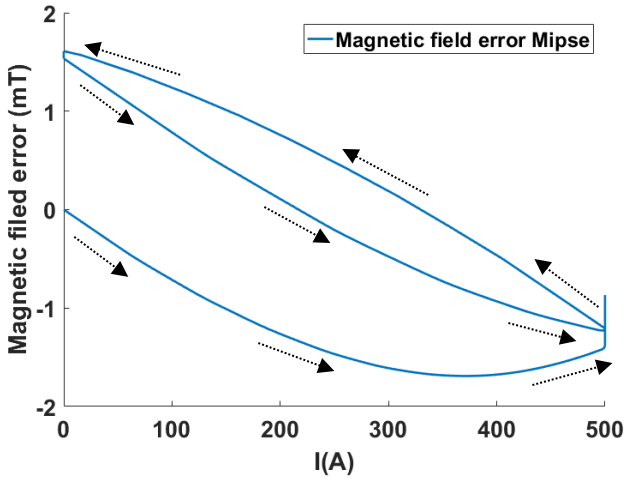

Figure 19. Magnetic field error from Mipse corresponding to screening current field at the coil center.

This hysteresis cycle corresponds actually to the Screening Currents Induced Field [17]. In our case with only screening current fields in width, the field hysteresis cycle is as expected counter clockwise.

3.4 Conclusion

In this part, we compared the simulations results with the experiment in terms of coil voltage and input energy, then we post process the modelling results to establish the energy balance of the coil, and from there derive the coil inductance variations. We were then able to propose and decompose of the coil voltage in an inductive and dissipative component.

4. Analysis of HTS coil behaviour using pick-up coils

Let us now discuss the results obtained using pick up coils, both as additional experimental validation of the modelling results, and as a way to get effective thermal runaway detection.

4.1 Pick-up and compensated voltage discussion

When using pick-up coils for compensation, we subtract their voltage v_{pick} to the coil voltage v_{sc} to get the compensated voltage (8), with k the adjustment factor of the compensation (representing the potentiometer).

$$v_{comp} = v_{sc} - k\, v_{pick} = v_{magnet} - k\frac{d\phi_{pick}}{dt} \quad (9)$$

For the Rogowski coil, ϕ_{pick} is the flux generated by the current in the current leads, proportional to di_t/dt and the compensated voltage is (9a), which we expect to stay constant throughout the ramps.

$$v_{pick} = M_{Rogowski}\frac{di_t}{dt} \quad \text{(10a)}$$

For the two pick-ups magnetically coupled to the HTS coil, ϕ_{pick} is the flux of the HTS coil passing through the pickup coil. Care must be taken when defining ϕ_{pick} in terms of mutual inductance. Even if the pickup coil inductance can be assumed constant, the HTS coil inductance is not, as we established in part 3. We must then consider the variation of M_{pick} with the time to get v_{pick} , which will then be varying during a ramp (9b). M_{pick} can be expressed through (10).

$$v_{pick} = M_{pick}\frac{di_t}{dt} + \frac{dM_{pick}}{dt}i_t \quad \text{(10b)}$$

$$M_{pick}(t) = k_{coupling}(t)\sqrt{L_{sc}(t).L_{pick}} \quad \text{(11)}$$

where $k_{coupling}$ is the coupling coefficient, that may vary between 0 and 1.

Similarly, to what was done in part 3 to evaluate the HTS coil equivalent inductance, we performed FEM magnetostatic simulations of the HTS coil and the two coupled pick-up coils for each time step in order to evaluate their mutual inductances with the HTS coil. A homogenous current distribution was assumed in the pick-up coils. The results are summarized Fig. 20 and Fig. 21 for the partially and fully coupled pick-ups respectively. As we saw previously in Tab. 1 the two coupled pick-up coils are much bigger (except for the co-wound Durnomag) in order to overcompensate the voltage REBCO coil. We find in Fig. 20 that the copper semi-coupled pick-up coil is higher than the REBCO coil (Fig. 15) as we desired.

The mutual inductance of the semi coupled coil is almost constant, which is explained by the fact that though the HTS coil inductance increase, the coupling coefficient actually decrease, from 0.363 to 0.357 during the ramp from 0 to 500 A.

On the contrary, for the fully coupled pick-up, the coupling coefficient increase during the ramp, from 0.97 at low current to 0.99 at 500 A.

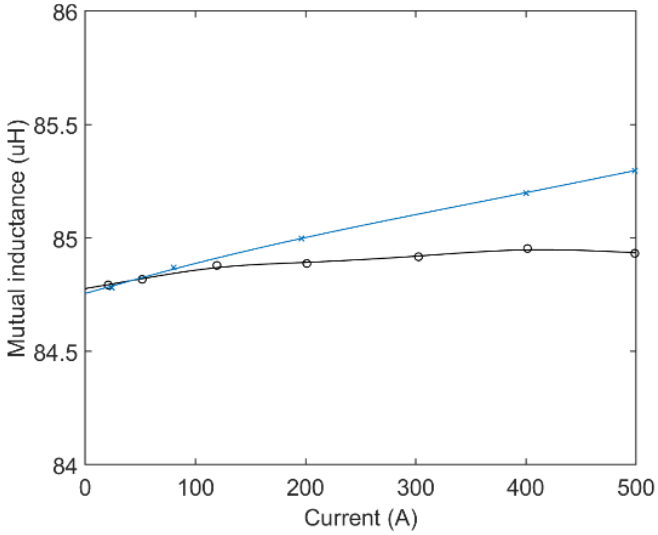

Figure 20. Mutual inductance of the partially coupled pick-up coil during first ramp (black) and second ramp (blue). Estimation based on simulation results

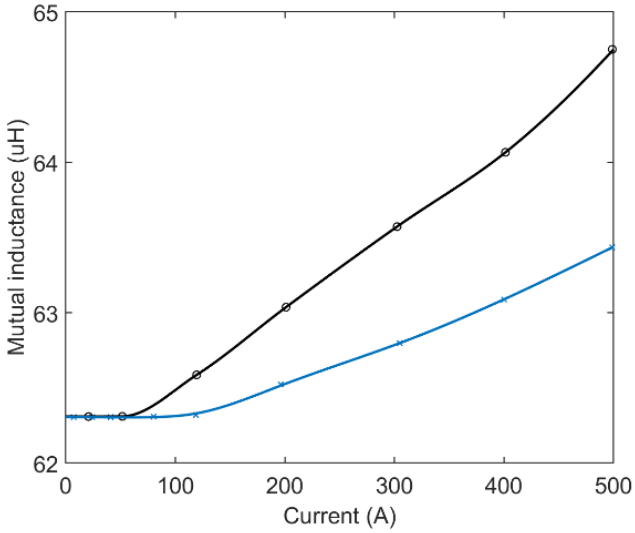

Figure 21. Mutual inductance of the very well coupled pick-up coil during first ramp (black) and second ramp (blue). Estimation based on simulation results

4.2 Experimental results

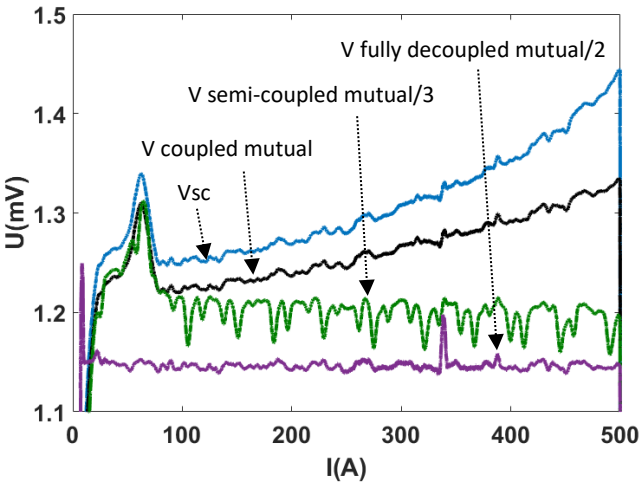

Figure 22. Voltages from the REBCO pancake (Vsc, light blue) and the 3 pick-up coils (V coupled mutual in black, V semi-coupled mutual/3 in green and V fully decoupled mutual/2 in purple) for the first current ramp up to 500 A.

Fig. 22 compares the compensated voltages of the three compensation coils to the REBCO coil voltage *Vsc*. They are labelled as "V coupled mutual" for the voltage on the co-wound pick-up coil, "V semi-coupled mutual" for the copper solenoid pick up placed below the REBCO coil and "V fully decoupled mutual" for the Rogowski coil. The graph does not start at zero to focus on the variation of the measured signals. For a better visualization we also divide the signals of the decoupled and the semi coupled pick-up coils by a factor of 2 and 3 respectively, as they were wound with too many turns.

As expected, the voltage on the fully decoupled pick up is constant during the ramp. The partially coupled pick up voltage is also almost constant as expected from the mutual inductance evaluation. It is even slightly decreasing.

The voltage on the co-wound pick-up is increasing during the ramp following a trend similar to that of Vsc, as expected.

If we adjust the compensation to cancel the REBCO coil voltage at zero current with the three pickup voltages we get the signals Fig. 23, where the drift of *Vsc* was also added for comparison.

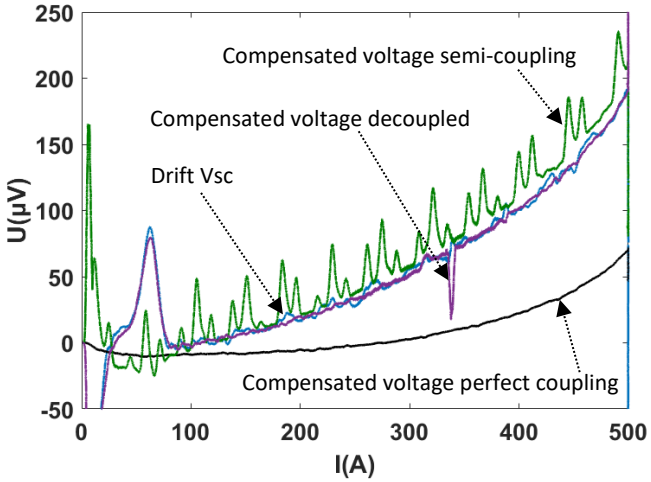

Figure 23. Compensated experimental voltages compared to the inductive drift from the REBCO pancake for the first current ramp up to 500 A. The compensated voltage of the perfectly coupled mutual is in black. The compensated voltage of the semi-coupled mutual in green as well as the compensated voltage of the decoupled mutual in purple merge perfectly with the REBCO coil voltage drift in light blue.

As expected, the decoupled pick up coil does not compensate the drift of *Vsc*. The partially coupled pick up coil does almost the same.

The very well coupled pick up on the opposite does compensate this drift significantly. At first sight, knowing that the coupling is very close to perfect in this last case, we may assume that the REBCO inductance drift is fully compensated and that what is left is the dissipating voltage we identified part 3. However, we can observe that the compensated voltage (in black) actually become smaller than zero in the 100 to 200 A range, which is unexpected.

The signals for the second ramp are showed Fig. 24 for the pick-up voltages and Fig. 25 for the compensated ones.

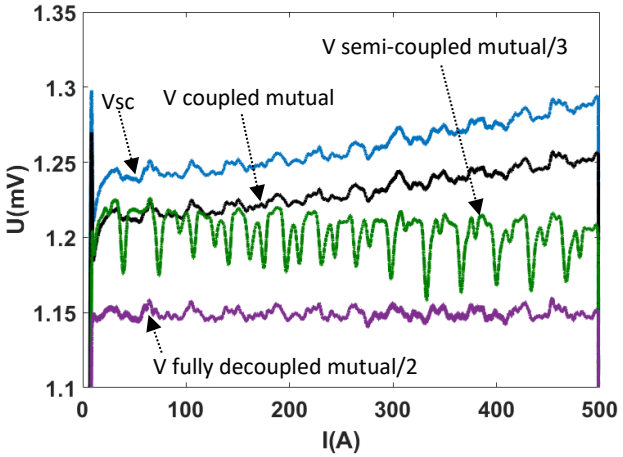

Figure 24. Voltages from the REBCO pancake (Vsc, light blue) and the 3 pick-up coils (V coupled mutual in black, V semi-coupled mutual/3 in green and V fully decoupled mutual/2 in purple) for the second and the following current ramp up to 500 A.

For the second ramp the compensated voltages from the Rogowski and the partially coupled solenoid are still mostly confused with the superconducting voltage drift but their drift is divided by 4 compared to the first ramp (Fig. 25). The compensated voltage from the fully coupled mutual inductance is very close to zero, as can be seen in more details Fig. 26.

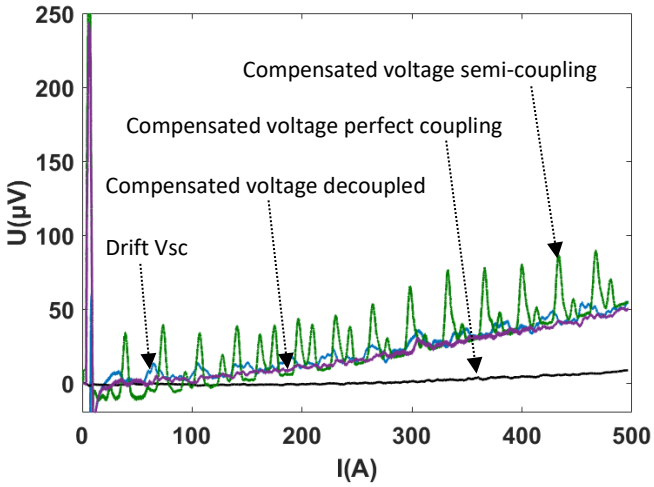

Figure 25. Compensated experimental voltages compared to the inductive drift from the REBCO pancake for the second and following current ramps up to 500 A. The compensated voltage of the perfectly coupled mutual is in black. The compensated voltage of the semi-coupled mutual in green as well as the compensated voltage of the decoupled mutual in purple merge perfectly with the REBCO coil voltage drift in light blue.

From a practical protection point of view these results can be summarized as follows:

- A partially coupled pick-up coil placed in the vicinity of the coil (with a 0.3 – 0.4 coupling coefficient) will compensate the REBCO coil transient voltage in the same way as an external Rogowski coil, but much easier to implement. The voltage drift of such compensated voltage is almost exactly that of the REBCO coil voltage itself, which we already discussed in part 3.
- A fully coupled co-wound pick-up coil compensate most of the REBCO coil voltage drift, especially for the second ramp (only 8 μV versus 50 μV for *Vsc*). It makes it much easier to detect early thermal runaway by mean of a low threshold. The signal also has much less perturbations. Its residual drift, though much smaller, is however not straightforward to interpret.

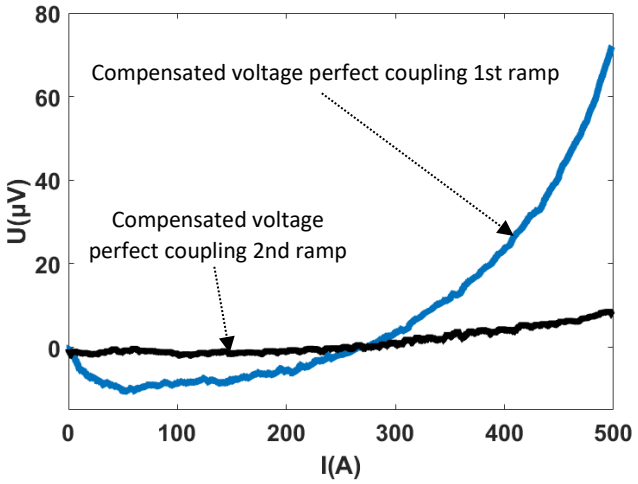

Figure 26. Comparison of compensated experimental voltage with a perfect coupling for a first (light blue curve) and second (black curve) current ramp up to 500 A.

4.3 Prediction of pick-up coil voltages and model validation

Based on the mutual inductances we evaluated in 4.1 and their time derivatives, we can predict the voltage of the coupled pick-up coils. Founded on our mutual inductance estimations, we expected the voltage for the semi-coupled pick-up to be constant. It is the case, though we did not predict the small decrease. The results for the fully coupled pick-up are more interesting. They are summarized Fig. 27, 28, 29. The rather good match between experimental and simulated voltages is a validation of our estimations for the pick-up coil mutual inductance and thus for the HTS coil equivalent inductance on which it is based.

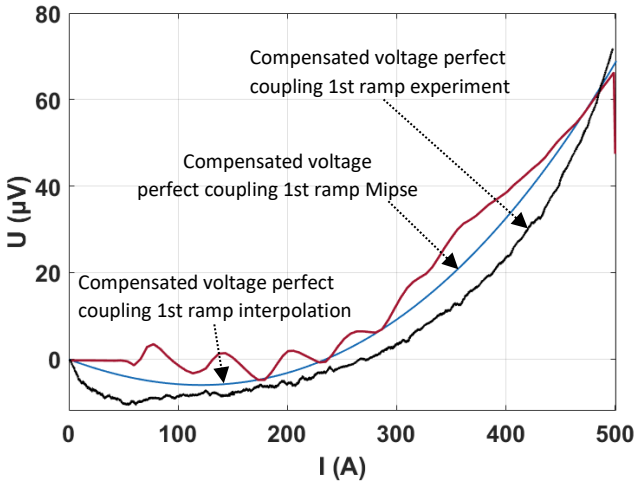

Figure 27. Compensated experimental voltage with the "perfect" coupling for the first current ramp up to 500 A compared to the modelling results. Experimental curve in black, Mipse curve in red and the interpolation in blue.

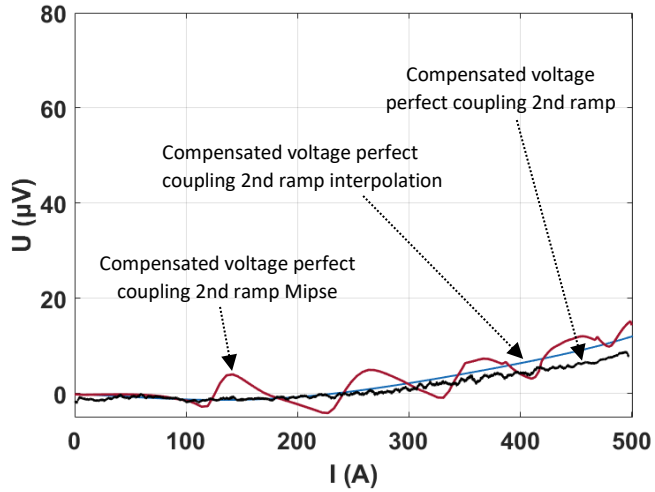

Figure 28. Compensated experimental voltage with a "perfect" coupling for the second current ramp up to 500 A compared to the modelling results. Experimental curve in black, Mipse curve in red and the interpolation in blue.

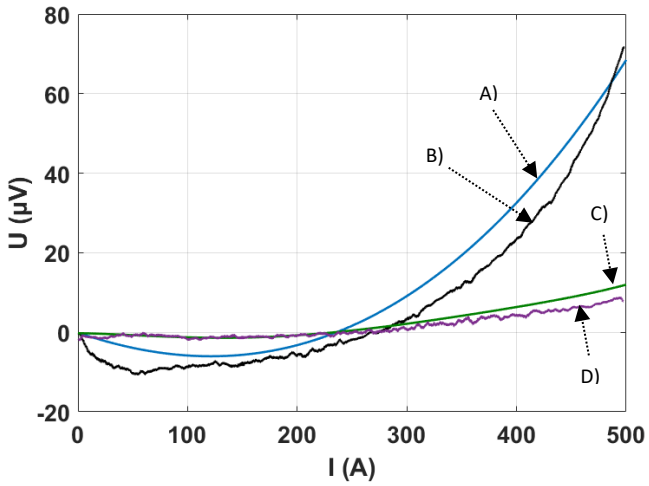

Figure 29. Compensated experimental voltage with a perfect coupling for a first and second current ramp up to 500 A compared to the interpolations from the modelling. A) Compensated voltage perfect coupling 1st ramp interpolation B) Compensated voltage perfect coupling 1st ramp experiment C) Compensated voltage perfect coupling 2nd ramp interpolation D) Compensated voltage perfect coupling 2nd ramp experiment. 1st ramp experimental in black and its interpolation in light blue. 2nd ramp experimental in purple and its interpolation in green.

5. Thermal runaway experiment

We now study the behavior close or slightly above Ic to investigate practically the early detection capability. We can see easily the voltage runaway due to overstepping Ic at 638 A Fig. 31. In terms of coil protection, we reach a high sensitivity: the threshold could have been set safely to about 150 µV for the Rogowski and the solenoid compensation pick-ups, and down to around 30 µV with the co-wound pick-up (Fig. 30-31).

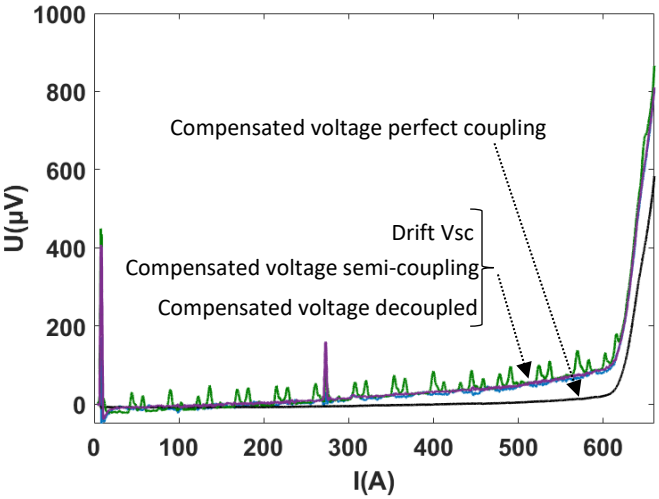

Figure 30. Compensated experimental voltages compared to the inductive drift from the REBCO pancake up to a runaway. The compensated voltage of the perfectly coupled mutual is in black. The compensated voltage of the semi-coupled mutual in green as well as the compensated voltage of the decoupled mutual in purple merge perfectly with the REBCO coil voltage drift in light blue.

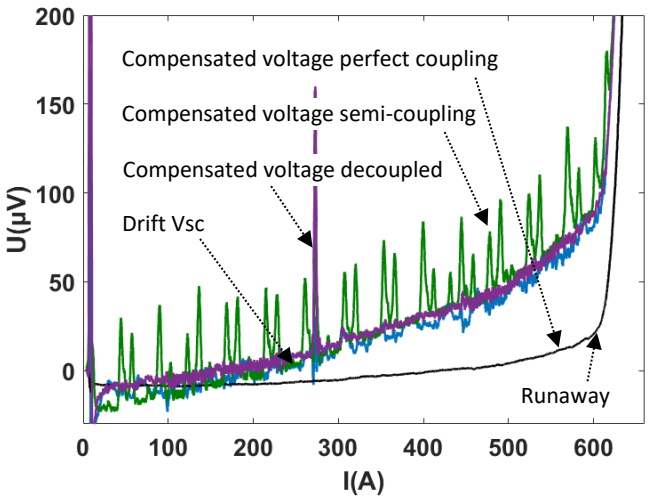

Figure 31. Zoom on compensated experimental voltages compared to the inductive drift from the REBCO pancake up to a runaway. The compensated voltage of the perfectly coupled mutual is in black. The compensated voltage of the semi-coupled mutual in green as well as the compensated voltage of the decoupled mutual in purple merge perfectly with the REBCO coil voltage drift in light blue.

The sensitivity can be further improved for the semi-coupled and decoupled cases by adapting dynamically the threshold with the signal drift, as this drift is accurately predicted by simulations, and remains the same throughout the life of the coil. The limit in this case would be the spike noise on the signals especially the semi-coupled one.

If we simulate a continuous ramp using the MIPSE model, the trend is similar to what was experimentally observed, with exponential voltage increase above 600 A. (Fig. 32). It demonstrates that the input data we used in the model are a good approximation of the tape that was used. The model, though not including thermal coupling predict accurately REBCO coil performances, at least if the dissipation level stays low.

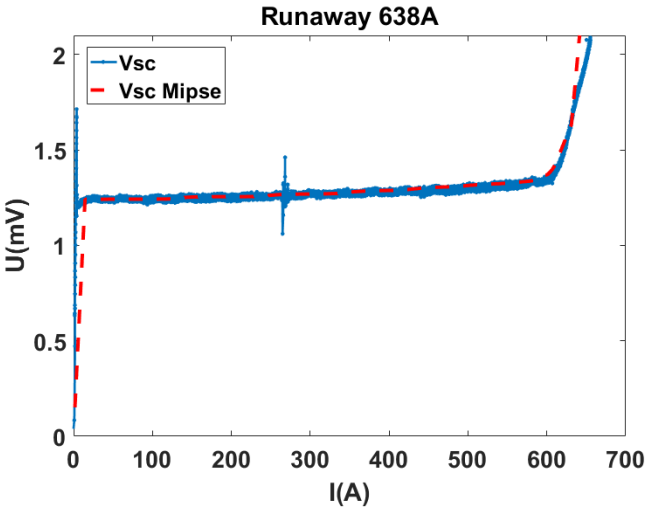

Figure 32. Comparison between the experimental runaway and the modelling from Mipse.

6. Other magnetic behaviours

When we first evaluated the coil, we actually ramped first to 100 A then discharged, and then gradually increased the target current by 100 A steps, each time going back to zero, until reaching the target current 500 A. Each time the previous current is overstepped, the voltage jumps suddenly up to a level corresponding to that of a first ramp to 500 A from a "virgin" state, while below the current previously reached it corresponds to that of a "second" ramp as presented previously (Fig. 33).

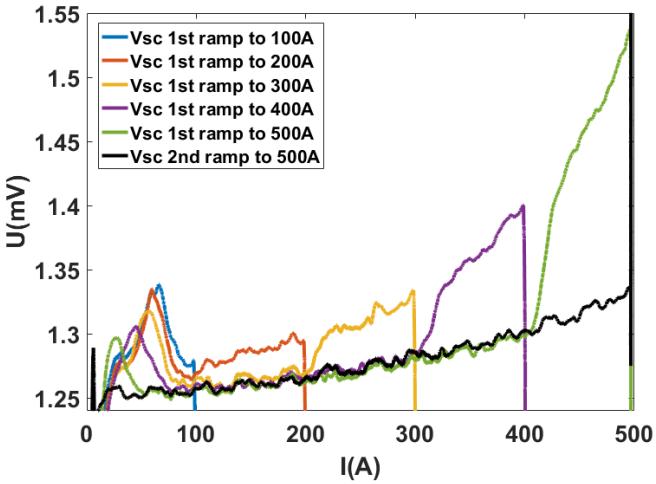

Figure 33. First current ramps by making steps from 100 amps up to 500 amps by going back to 0 and a second ramp up to 500 A.

At the beginning of every ramps we also notice a spike or "bump" on the coil voltage. This bump is reduced as we ramp each time to a higher current, until disappearing when we reached a current close to the coil critical current (Fig. 34). Currently, we don't know exactly the origin of this behaviour, which is not reproduced by the model. We can establish that it is magnetic since we can see similar bumps on the voltage of both the co-wound and the semi-coupled compensation coils. We will investigate this phenomenon on future test campaigns on other REBCO coils.

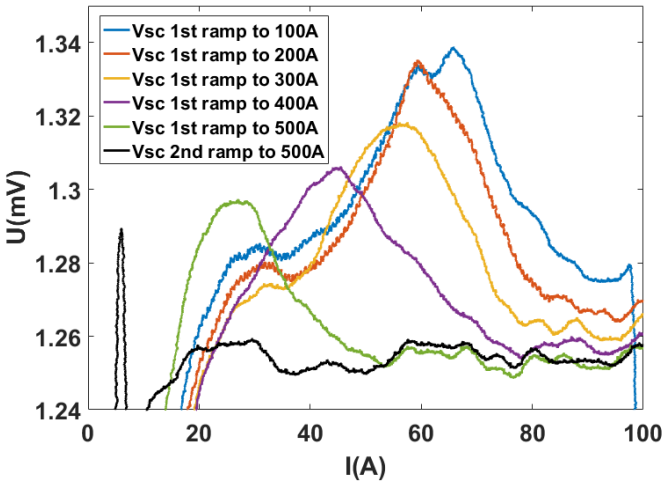

Figure 34. Unknown magnetic bump decreasing as we get closer of the coil critical current.

7. Conclusion and prospect

In this work we studied the transient behaviour of a small REBCO coil, thanks to three pick up coils whose magnetic coupling with the REBCO coil varies from zero to close to one. Using transient electromagnetic simulations, we were

able to quantify the contributions of inductance variation and transient losses on the coil voltage during ramp up, and propose an estimation of the dynamic variation of the coil inductance. We were able to validate this estimation of the inductance, and thus the modelling approach, by using it to predict pick-up coil voltages.

From a practical point of view, we observed that a conventional pick up coil with partial coupling for compensation could be used to get a high thermal runaway detection sensitivity. The detection sensitivity increases if we adapt the threshold dynamically during the ramp based on the expected drift, which can be obtained from simulation results beforehand. This is the solution we consider for future large scale REBCO coils, and that we already used for testing numerous double pancakes in the ongoing BOSSE project [10,18,19].

The thermal runaway detection sensitivity can be improved even further using a co-wound pick up coil, which reduces noise and drift. The solution tested here is a co-wound high strength / high resistivity tape. This solution is particularly appealing applications where the mechanical stress is very large, like high field (or high flux) solenoids, where such tape is already used both as mechanical reinforcement and insulation [4, 20].

The possibility to use the co-wound metallic tape of metal-as-insulation (MI) coils as a type of pickup coil in spite of the electrical contact with the REBCO tape needs to be investigated, as it could give access to small REBCO coil effective inductance variations and thus provide very early warning of the coil limits.

Acknowledgements

We would like to thank the MAGE team from G2Elab and particularly Ramdane Brahim and Meunier Gérard for their work on Mipse.

References

[1] Yasuyuki Miyoshi, Arnaud Badel, Xavier Chaud, Tara Benkel, Benjamin Vincent, Pascal Tixador, Julien Marpaud, François Debray, Thibault Lécrevisse, Mélanie Devaux, Philippe Fazilleau, and Jean-Michel Rey 2015 Performance Tests of Prototype High-Field HTS Coils in Grenoble *IEEE Trans. Appl. Supercond.* 25 4600505

[2] T. Lécrevisse, X. Chaud, F. Debray, M. Devaux, P. Fazilleau, F. P. Juster, Y. Miyoshi, J.-M. Rey, P. Tixador, and B. Vincent 2013 Quench Propagation in YBCO Pancake: Experimental and Computational Results *IEEE Trans. Appl. Supercond.* 23 4601805

[3] Hahn S, Park D K, Bascunan J and Iwasa Y 2011 HTS pancake coils without turn-to-turn insulation IEEE Trans. Appl. Supercond. 21 1592 – 1595

[4] Lécrevisse T and Iwasa Y 2016 A (RE)BCO pancake winding with metal-as-insulation IEEE Trans. Appl. Supercond. 26 4700405

[5] Wang Y, Chan W K and Schwartz J 2016 Self-protection mechanisms in no-insulation (RE)Ba2Cu3Ox high temperature superconductor pancake coils Supercond. Sci. Technol. 29 045007

[6] Song J-B, Hahn S, Lécrevisse T, Voccio J, Bascuñán J and Iwasa Y 2015 Over-current quench test and self-protecting behavior of a 7 T/78 mm multi-width no-insulation REBCO magnet at 4.2 K Supercond. Sci. Technol. 28 114001

[7] Arnaud Badel , Blandine Rozier , Kohki Takahashi , and Satoshi Awaji 2019 Simulation of Local Dissipation Phenomena in the REBCO Insert of the 25-T CSM Magnet: Understanding and Preventing Destructive Thermal Runaway *IEEE Trans. Appl. Supercond.* 29 4600605

[8] Arnaud Badel, Tatsunori Okada , Kohki Takahashi , Shinji Fujita , Hiroshi Miyazaki , Shigeru Ioka, and Satoshi Awaji 2021 Detection and Protection Against Quench/Local Thermal Runaway for a 30 T Cryogen-Free Magnet *IEEE Trans. Appl. Supercond. 31* 4700705

[9] Arnaud Badel, Blandine Rozier, Brahim Ramdane, Gérard Meunier and Pascal Tixador 2019 Modeling of 'quench' or the occurrence and propagation of dissipative zones in REBCO high temperature superconducting coils *Supercond. Sci. Technol.* 32 094001

[10] Julien Vialle, Arnaud Badel , Pascal Tixador, Jeremie Ciceron , Frederick Forest, and Raphaël Pasquet 2021 Preliminary Tests of Pancakes From a 12 T REBCO insulated Solenoid Magnet *IEEE Trans. Appl. Supercond.* 31 4600805

[11] Rozier Blandine, Badel Arnaud, Ramdane Brahim and Meunier Gérard 2019 Calculation of the local current density in high-temperature superconducting insulated rare earth–barium–copper oxide coils using a volume integral formulation and its contribution to coil protection *Supercond. Sci. Technol.* 32 044008

[12] H. W. Weijers et al., "Progress in the Development of a Superconducting 32 T Magnet With REBCO High Field Coils," in IEEE Transactions on Applied Superconductivity, vol. 24, no. 3, Art no. 4301805, 2014.T.

[13] Ariyama, T. Takagi, D. Nakayama, E. Sasaki, T. Takao, O. Tsukamoto, and T. Matsuoka, “Quench Protection of YBCO Coils: Co-Winding Detection Method and Limits to Hot-Spot Temperature” IEEE TRANSACTIONS ON APPLIED SUPERCONDUCTIVITY, VOL. 26, NO. 3, APRIL 2016, 4702205

[14] Dixon, I. R., et al., “The 36-T Series-Connected Hybrid Magnet System Design and Integration,” IEEE Transactions on Applied Superconductivity, v 27, n 4, June 2017, 4300105.

[15] Martovetsky, N. N., Chaplin, M. R., “Detection of the normal zone with cowound sensors in cable-in conduit conductors,” IEEE Transactions on Applied Superconductivity, v 7, n 2 pt 1, p 451-454, June 1997.

[16] G2ELab 2018 MIPSE : Modeling of Interconnected Power SystEms https://g2elab.grenoble-inp.fr/en/platforms/mipse-modeling-of-interconnected-power-systems-1 (accessed 8 April 2021)

[17] Tara Benkel, Yasuyuki Miyoshi, Guillaume Escamez, Daniel Gonzales, Xavier Chaud, Arnaud Badel, and Pascal Tixador 2016 REBCO Performance at High Field With Low Incident Angle and Preliminary Tests for a 10-T Insert *IEEE Trans. Appl. Supercond.* 26 4302705

[18] Guillaume Dilasser, Philippe Fazilleau, and Pascal Tixador 2017 Experimental Measurement and Numerical Simulation of the Screening Current-Induced Field Decay in a Small ReBCO Coil *IEEE Trans. Appl. Supercond.* 27 4900104
[19] Jeremie Ciceron;Arnaud Badel;Pascal Tixador;Frederick Forest 2017 Design Considerations for High-Energy Density SMES *IEEE Trans. Appl. Supercond.* 27 5700705
[20] Jeremie Ciceron;Arnaud Badel;Pascal Tixador;Raphaël Pasquet;Frederick Forest 2018 Test in Strong Background Field of a Modular Element of a REBCO 1 MJ High Energy Density SMES *IEEE Trans. Appl. Supercond.* 28 5701005
[21] J. Lu, H. Kandel, K. Han, W. R. Sheppard, D. M. McRae, A. Voran, K. W. Pickard, R. E. Goddard, Y. L. Viouchkov, H. W. Weijers, and W. D. Markiewicz, “Insulation of coated conductors for high field magnet applications,” IEEE Trans. Appl. Supercond., vol. 22, no. 3, Art. no. 7700304, 2012.